Quantification of Interfacial Motions Following Primary and Revision Total Knee Arthroplasty: A Verification Study versus Experimental Data

Quantification of Interfacial Motions Following Primary and Revision Total Knee Arthroplasty: A Verification Study versus Experimental Data.

Noel Conlisk, BEng (Hons), PhD[1, 2],

Colin R. Howie, BSc, MB ChB, FRCS Ed (Orth)[1,3],

Pankaj Pankaj, BTech, ME, PhD[2],

Running title: Post-TKA motions using verified models.

[1]School of Clinical Sciences, The University of Edinburgh, Edinburgh, UK

[2] School of Engineering, The University of Edinburgh, Edinburgh, UK

[3] Department of Orthopaedics, New Royal Infirmary of Edinburgh, Old Dalkeith Road, Little France, Edinburgh, UK

Author contributions:

Noel Conlisk: Writing the manuscript, Main author, Study design, Data collection/Analysis.

Colin R. Howie: Writing the manuscript, Study design, Support and guidance during study.

Pankaj Pankaj: Writing the manuscript, Study design, Support and guidance during study.

Correspondence:

Dr. Noel Conlisk
Room E3.24,
The Queen's Medical Research Institute,
College of Medicine and Veterinary Medicine,
The University of Edinburgh,
EH16 4TJ, Edinburgh, UK
Phone: (+44) 7775 332506
Email: noel.conlisk@ed.ac.uk

ABSTRACT

Motion at the bone-implant interface, following primary or revision knee arthroplasty, can be detrimental to the long term survival of the implant. This study employs experimentally verified computational models of the distal femur to characterise the relative motion at the bone-implant interface for three different implant types; a posterior stabilising implant (PS), a total stabilising implant (TS) with short stem (12mm x 50mm), and a total stabilising implant (TS) with long offset stem (19mm x 150mm with a 4mm lateral offset). Relative motion was investigated for both cemented and uncemented interface conditions. Monitoring relative motion about a single reference point, though useful for discerning global differences between implant types, was found to not be representative of the true pattern and distribution of motions which occur at the interface. The contribution of elastic deformation to apparent reference point motion varied based on implant type, with the PS and TSSS implanted femurs experiencing larger deformations (43 μm and 39μm respectively) than the TSLS implanted femur (22 μm). Furthermore, the pattern of applied loading was observed to greatly influence location and magnitude of peak motions, as well as the surface area under increased motion. Interestingly, the influence was not uniform across all implant types, with motions at the interface of long stemmed prosthesis found to be less susceptible to changes in pattern of loading. These findings have important implications for the optimisation and testing of orthopaedic implants *in vitro* and *in silico*.

KEYWORDS: Micromotion; Stemmed vs. Stemless TKA; Finite element analysis; In vitro experiments; bone-implant interface.

1. INTRODUCTION

Aseptic loosening is recognised as one of the predominant causes of revision total knee arthroplasty (TKA) globally [1-5]. Loss of fixation through aseptic loosing can lead to pain, malalignment of the prosthesis and eventual failure. The three main causes of aseptic loosening are particle induced osteolysis due to excessive wear of the articular surfaces [6], bone loss due to periprosthetic stress shielding, and fibrous tissue formation instead of bone ingrowth as a result of relative motion at the bone prosthesis interface [7].

Changes in the position and orientation of an implant over time are measured clinically through examination of X-rays or by specialist techniques such as radio stereo photogrammetric analysis (RSA). While RSA offers a significant improvement in measurement accuracy over X-rays (approximately ten times greater) [8-11] it also has some limitations. Primarily, RSA can only track large changes (e.g. > 100μm) in the position of the prosthesis [11-14]. As these methods are unable to capture the small but repetitive inducible motions (e.g. <40μm) which play a key role in particle induced osteolysis [9] and aseptic loosening of the implant surgeons increasingly rely on *in vitro* [15-25] laboratory testing and *in silico* modelling [15-17, 26-29] to supplement clinical knowledge on motion at the interface and overall implant stability.

Loading at the knee joint and in particular the articular surface of the distal femur is complex. Multiple components of force act in multiple directions (e.g. tibio-femoral force, anterior-posterior shear force and patella-femoral force), the magnitude, position and orientation of which can change dramatically over the course of a gait cycle and indeed with different patterns of gait [30-32]. Furthermore, the joint itself is stabilised throughout its range of motion by numerous muscles and ligaments. All these factors make replication of *in vivo* loading conditions extremely challenging *in vitro* without the aid of expensive specialist equipment [33], as such many

previous studies have employed simplified loading conditions to examine interfacial motion [18, 21, 34, 35]. However the influence of such simplifications on predicted motions at the interface following total knee replacement has not been widely assessed. Only one previous study [26] has attempted to address this issue directly. In their study, Berahmani and colleagues examined the micromotion characteristics of a single cruciate retaining implant, and found that simplifications in applied loading could lead to overestimation of peak motions by up to 22%.

Due to the complexity of the region of interest and its changing contact area with flexion, direct access to the bone-implant interface is often not possible *in vitro*, as a consequence many experimental setups rely on monitoring interfacial motions indirectly from sensors positioned at a small distance away from the interface [16, 18-20, 25, 36]. However, such approaches are subject to the inclusion of a number of flexibilities (e.g. bending, and elastic deformation of the bone) which may lead to large errors. Thus far, only a limited number of studies have attempted to directly quantify the impact of elastic deformations on reported results [21, 28, 36, 37], others tend to focus instead on long term indicators such as permanent migration, which is said to be less sensitive elastic deformation of the bone [19, 20, 36].

Little consensus exists on the exact contribution of elastic deformations to errors in *in vitro* measurements. Gilbert et al. [38] suggested that the contribution was quite low ($3-15\mu m$) in comparison to values of micromotion observed. Monti et al. [37] reported elastic deformations of $2.3\mu m$ at the interface, however, these values were found to increase almost linearly with increasing distance from the interface. Distally, a study by Moran [21] found that elastic deformations alone could account for measured motions of up to $50\mu m$ in cancellous bone structures following TKA. The combination of motion and deformation may lead to experimental values overestimating the true level of motion at the interface [28], which could

obscure important inter-implant trends.

Therefore the aims of this study were:

- To verify the behaviour of the finite element (FE) models against data from an earlier in vitro study [18], and then use these models to investigate what contribution elastic deformation of the underlying bone might have on motions recorded in all six degrees of freedom about a central reference point.
- To examine if the magnitude of elastic deformations varies with varying implant type.
- To determine how representative global reference point motions are of the motions obtained directly at the interface numerically.
- To examine how predicted interfacial motions change in response to changes in the pattern of loading applied to the femur.

2. METHODS

This study combined experimental data and FE models to investigate the relationship between measurements of relative motion obtained *in vitro* and numerically. In this study, all FE analyses were conducted in Abaqus (Abaqus 6.10-1, Dassault Systemes, Simulia, Providence, RI, USA).

2.1 Finite element model setup:

2.1.1 Geometry:

All models in this study were constructed from a virtual representation of the large left composite femur (Sawbones; Pacific Research Laboratories, Vashon, Washington) and implanted with three different implant types from the Triathlon® series (Stryker®, Newbury, United Kingdom) as shown in Fig. 1; a posterior stabilising implant (PS), a total stabilising implant (TS) with short stem (12mm x 50mm), and a total stabilising implant (TS) with long offset stem (19mm x 150mm with a 4mm lateral offset). Computer aided design software (Autodesk Inventor™ 2010, Autodesk Inc., San Rafael, CA) was used to develop 3D models of each implant investigated, and to carry out surgical resections on the femur for virtual implantation. To ease computational costs and avoid projecting bad elements some simplifications of small sharp features on the implant and stem surfaces were considered (e.g. smoothing of the thin flutes along the length of the stem, and removal of screw threads at modular junctions).

To incorporate identical loading and boundary conditions to the *in vitro* study [18] necessitated the inclusion of a stiff steel plate through which the machine load could be applied, and a ultra-high-molecular-weight-polyethylene (UHMWPE) tibial bearing insert with central post and a conforming articulation surface to allow load transfer to the femur, as shown in Fig. 2a.

2.1.2 Interface conditions:

Frictional interfaces were applied to both the bone-prosthesis and prosthesis-prosthesis interfaces to replicate the uncemented *in vitro* trials. Coulomb friction was implemented at all bone-prosthesis interfaces, with a frictional coefficient of $\mu = 0.3$, representing an average of the reported values in literature [15, 39-41].

Knowledge of several additional software specific parameters is required to ensure frictional analyses conducted in Abaqus are easily replicable, to this end, details of these parameters and their respective values are provided in the supplementary text (Supplement A).

Additionally, a second set of models were created which employed tied constraints at the bone-prosthesis interface to simulate the effects of femoral component cementing and to allow quantification of elastic deformations. A summary of all interface conditions is presented in Table 1.

2.1.3 Material properties:

Linear elastic isotropic material properties were applied to bone [42] and implant structures, where implant and offset adapter/femoral stem structures were composed of cobalt chromium (CoCr) and titanium (ti-6al-4v) respectively, and the tibial insert was composed of UHMWPE. The material properties applied to each structure are presented in Table 2.

2.1.4 Loading:

To remain consistent with the experimental loading protocols for 20° flexion described in Conlisk et al. [18], a cyclical load was applied to the centre of the steel plate (representative of the load cell attachment site), this load was set to vary from 0N to 1643N during the first cycle and 20N to 1643N during subsequent 39 cycles to maintain contact between tibial insert and

femoral component, as in the *in vitro* testing protocol.

All 40 cycles were carried out during a single static load step in Abaqus. This was achieved by varying the load through a custom amplitude curve and then defining output of all interface parameters and displacements at each full time increment. A series of predefined time points were used to ensure all stages of each loading peak would be captured during the analysis.

After verification of the FE models under experimental conditions, additional simulations were then undertaken to examine the effects of more realistic loading pattern on motion at the bone-prosthesis interface. In contrast to the *in vitro* loading conditions, the physiological loading conditions consisted of six components of force applied directly to the femoral component: the patella-femoral force (PF); the medial and lateral components of the joint normal force (Fm and Fl); the medial and lateral components of the joint shear force (APm and APl); and the internal/external moment (IE). To avoid issues of point loading, computationally the IE moment was included in the model by adjusting the values of APm and APl (which act perpendicular to the joint normal force) applied to the femur to induce the desired moment. It is important to note that the sum of the forces in the AP direction was not altered through this method. The magnitudes of loading used for 20° flexion were derived from literature [30, 32] and are presented in Table 3. To remain consistent with the FE model based on the experimental study, the location and surface areas of loading resulting from the action of the tibial insert on the femoral component were transferred across to the physiological model. It should be noted that the maximum tibio-femoral force was the same under both loading conditions.

2.1.5 Boundary conditions:

The femur was truncated at the mid-shaft and fully fixed in all degrees of freedom on the

proximal most surface. Additionally the steel plate was restrained such that only the degree of freedom relating to compression of the plate on the femur was free, mimicking the experimental setup.

Final FE meshes typically comprised of approximately 400,000 linear tetrahedral elements (C3D4). To ensure accuracy of the numerical solution, a maximum allowable element edge length of 2mm was applied to all models. Based on convergence checks, a further reduction in edge length produced a negligible (2%) change in the calculated displacements and stresses, while dramatically increasing simulation runtime. Simulation runtime for each model was approximately 2hrs on a dual core Intel i5 laptop with 8GB of ram.

2.2 Comparison of *in vitro* and FE micromotion measurements:

The apparatus and experimental protocol referred to in this study has been described in detail previously [18]. In brief, a custom test rig using an array of six differential variable reluctance transducers (DVRTs) was developed, and attached to the bone-implant construct (Fig. 2a). This permitted recording of relative translational and rotational motions of the implant to the bone, in all six degrees of freedom about a reference point close to the interface (Fig. 2c). When comparing measurements taken during *in vitro* experiments to those in an FE model it is essential that the same parameters be measured in the same manner, to this end it was necessary to recreate the sensor placement and setup used in the *in vitro* experiments. Rather than adding to model complexity and runtime by explicitly modelling the entire three dimensional test rig, the location of each sensor and its corresponding target were recreated virtually using a system of reference points and coupling constraints, as shown in Fig.2b. In this manner, the displacement of the sensor could be approximated by calculating the relative change in position of the target

sphere reference point to its corresponding sensor reference point. It can be seen from Fig. 2b that the displacement profile of DVRTs 1-3 are approximated by calculating the relative nodal displacement of the sphere C reference point and corresponding sensor housing reference point in the global x, y, z coordinates over the course of the 40 cycles. Similarly DVRTs 5 and 6 displacements are determined by comparing relative nodal displacement in the y and z directions of the sphere B reference point, and DVRT 4 by comparing relative nodal displacement in the z direction only of the sphere A reference point.

Once the characteristic displacement curve for each sensor was extracted from the FE model (see example curve, supplement B Fig. B.1) this data was collectively exported and analysed using the same custom LabVIEW^{TM} programs developed in the previous *in vitro* study [18]. Thus, allowing the relative inducible motions of the femoral component to the bone at the central implant reference point to be determined. An overview of the results processing workflow is presented in Fig. 3.

2.3 Characterisation of motion directly at the interface:

Motion predicted directly at all points of the interface were quantified using three inbuilt parameters in Abaqus; Copen, Cslip1, and Cslip2. Where Copen represents the normal distance by which the contacting surfaces have separated (henceforth referred to as gap opening), and Cslip1 and Cslip2 represent motions which act tangential to the contacting surfaces (henceforth referred to as shear micromotions) in direction 1 and 2, these directions being orthogonal to each other. These motions were then visualised as colour contour plots. The corresponding surface area associated with six different bands of shear micromotion (0 – 20μm, 20 – 40μm, 40 – 60μm, 60 – 80μm, 80 – 100μm and 100 – 150μm) was also calculated using code developed in-house.

3. RESULTS

3.1 Comparison of *in vitro* and FE results:

This first set of results focuses on comparison of the output from the FE models to that of the *in vitro* experiments for the same reference point, under both uncemented and cemented interface conditions. The overall magnitude of translational motions for each implant type, under both interface conditions is presented in Fig. 4, alongside the corresponding *in vitro* results. The dashed orange lines represent the range of motions at which fibrous tissue formation may occur. From Fig. 4a it can be seen that a $< 40 \mu m$ difference is observed between *in vitro* and FE results. This difference reduces even further for cemented cases ($< 16 \mu m$). These differences likely arise from variations in the individual components of motion (Supplement B), possibly due to slight differences in implant fit between experimental and FE setups. However, it is important to note that the predicted FE motions are of the same magnitude and within the ranges observed *in vitro*. Furthermore, the overall global trends are found to be similar, e.g. motion reduces in the presence of stemmed prostheses, and with cemented interfaces.

3.2 Quantification of elastic deformations:

The FE simulations employed two different conditions at the interface modelling uncemented and cemented (frictional and tied) fixation of the implants. In tied simulations, numerically no relative motion is permitted to occur at the bone-implant interface. Therefore, any motions or rotations recorded about the reference point in these situations represent the contributions of elastic deformation rather than true interfacial motion. From Fig. 4b, it can be seen that the contribution of elastic deformation to reference point motion varies based on implant type, with the PS and TSSS implanted femurs experiencing larger deformations (43 μm and 39μm

273 respectively) than the TSLS implanted femur (22 μm). This is likely due to the added stiffness of
274 the long stem which anchors the implant in position and resists deformation of the underlying
275 cancellous bone under loading.

276 3.3 Comparison of reference point and interface motion:

277 On investigation of the predicted motions directly at the interface using contour plots (Fig. 5a
278 and Fig.5b), it can be seen that motion is distributed in a complex manner over the multi-planar
279 surface. In all cases motions favourable for bone ingrowth [43], and well below those predicted
280 at the reference point, are observed on the distal surface, anterior chamfer and posterior chamfer
281 ($<40\mu m$). However, on the anterior and posterior surfaces motions in excess of $60\mu m$ and
282 $100\mu m$ respectively are observed in certain regions near the edges of the implant. These findings
283 highlight the inability of a single point to capture the complex behaviour of the interface.

284

285 3.4 Influence of applied loading pattern:

286 When a more physiologically realistic arrangement of forces is applied to the distal femur, the
287 pattern and distribution of motion (Fig. 6) differs considerably from that experienced under *in*
288 *vitro* loading conditions (Fig. 5). Peak shear micromotions for the PS and TSSS implanted
289 femurs are found to slightly increase in direction 1 (Cslip1) under physiological loading
290 conditions (by $2.24\mu m$ and $9.60\mu m$ respectively). On the other hand, peak shear micromotions
291 in direction 2 (Cslip2) for all implant types are found to reduce by an average of $16\mu m$ (Table 4).
292 The surface area associated with motion in the range of $20-80\mu m$ increases dramatically under
293 physiological loading conditions (Table 5). Interestingly, at higher bands of motion (e.g.
294 $80-100\mu m$ and $100-150\mu m$), the surface area associated with increased motion is substantially
295 reduced relative to that experienced under simplified loading conditions.

4. DISCUSSION

This study presented the use of experimentally verified finite element models of the distal femur, implanted with primary and revision femoral components, to investigate and quantify relative motions and elastic deformations at the bone-implant interface.

Predicted (FE) and measured (*in vitro*) translational and rotational relative motions for both frictional (supplement B: Table 1) and tied (supplement B: Table 2) interface conditions were found to be within the same range, however, directional differences between the largest components of motion measured in the *in vitro* experiments and that of the FE models were observed in the present study, as has been the case in similar studies of this nature [16, 44]. Similar to that found by Conlisk et al. [18], translational and rotational components of relative motion were predicted to be smallest in the TS implant with long offset stem. Differences in PS and TS (short stem) implanted femurs under frictional conditions were very small. The component of rotation found to be smallest in general was θ_z. The percentage reduction in motion observed going from a fully frictional to fully tied interface was found to be similar to *in vitro* conclusions on uncemented and cemented implant motions. The overall trends evident by comparing Fig. 4a and Fig. 4b lend support to the idea that comparable implant performances can be achieved without the use of stems provided full fixation of the implant is achieved at the metaphysis [18].

Based on the assumption that no motion is permitted at the bone-implant interface of cemented FE models (due to tied constraints), we can then approximate the magnitude of the elastic deformations acting on each implanted femur through examination of apparent motions at the reference point for the “cemented” FE scenarios. In the present study such quantities are estimated to account for readings ranging from $1-39\,\mu m$ depending on implant and direction of

motion. These values are within the range previously reported by Moran [21] and significantly higher than that observed in the hip [37, 38]. These findings show that elastic deformations can still greatly influence reference point motion [28], despite close positioning of the test rig to the bone-implant interface. It is important to note that knowledge of the elastic deformations, in addition to interfacial motion, may be of relevance during long term tests [19], as any increase in the combined motion/deformation may indicate an increased risk of fatigue damage to the underlying bone [45]. Reassuringly, after adjusting for the specific contribution of elastic deformations for each implant type, motions about the reference point were still found to follow the same general trends, highlighting that such comparative *in vitro* studies can still provide meaningful information on the differences in global behaviour observed between implant types. However, if attempting to adjust for the contribution of elastic deformations, future studies should bear in mind that different implant configurations will be subject to different levels of deformation, as has been shown in the present study (e.g. largest elastic deformations in PS implanted femur, and smallest in TS implanted femur with long offset stem).

Similar to Tarala et al. [28], this study has also shown that motion of the reference point does not reflect the complex behaviour of interface. On investigation of the true predicted interfacial motions using contour plots (Fig. 5), results are observed to be lower than that predicted about the reference point, typically $< 40 \mu m$ on the distal surface, but rising much higher on the anterior and posterior surfaces. This indicates that while *in vitro* investigations using the current DVRT setup may be useful for providing a general comparison of overall component stability, they are not fully able to characterise the complex interactions taking place directly at the interface. Similar limitations with respect to investigation of motion following THA of the femur and TKA of the tibia have been previously reported [16, 28].

342 In a recent FE study by Berahmani et al. [26], the influence of different loading configurations
343 on micromotion at the bone-implant interface following primary TKA with a cruciate retaining
344 implant was examined. Similar to the finding of the present study, Berahmani and colleagues
345 reported that simplified loading conditions and a lack of patella-femoral force caused an
346 overestimation of micromotion at the interface. In their study it was also suggested that the
347 distribution of motions was quite similar regardless of the loading configuration applied.
348 However, in the present study, application of complex physiological loading patterns over a
349 simple tibio-femoral force pattern (often applied *in vitro*) not only led to alterations in magnitude
350 and location of peak motions, but also markedly changed the distribution of motions over the
351 entire interface [16]. Interestingly, the effect of loading on motions was not uniform across
352 different implant types, with motions at the interface of long stemmed implants found to be less
353 susceptible to changes in loading pattern. One possible explanation for the discrepancy in
354 findings between the two studies is a difference in medial-lateral load distribution (M-L). In
355 Berahmani et al. the M-L distribution was kept constant for both simplified and full loading
356 conditions, whereas, in the present study the M-L distribution of the tibiofemoral force was 51%-
357 49% while replicating the *in vitro* conditions and 60%-40% under physiological loading
358 conditions. This along with other factors, such as implant geometry and modelling parameters
359 selected (e.g. frictional coefficients, and applied loads) may also explain why, contrary to that
360 reported by Berhamani et al. [26] the distal surface and anterior chamfers were found to exhibit
361 high levels of micromotion under complex loading conditions.
362 This study has some limitations. One potential limitation lies in the fact that no interference fit
363 was modelled between the implant and the bone for the frictional cases, as this parameter was
364 not recorded during the experiments it adds another element of uncertainty when trying to

365 replicate them *in silico*. While the magnitude of motions may reduce with press-fit [15]. It is
366 unlikely that the main trends observed here, in relation to the quantification of elastic
367 deformations and the role of applied loading on magnitude and distribution of motion, would
368 change given the comparative nature of this study.

369 Despite efforts taken to accurately replicate *in vitro* conditions *in silico*, this study showed that *in*
370 *vitro* measurements of motion did not match perfectly with FE predicted motions. These
371 differences in magnitude of translational and rotational relative motions may be explained by
372 both geometrical issues (e.g. ideal Boolean fit in FE vs. imperfect fit *in vitro*) and interface issues
373 (e.g. frictional properties applied numerically). To minimise errors future tests should closely
374 calibration bone-implant interface frictional properties based on benchmark tests with samples
375 from physical lab specimens of all relevant materials. Furthermore, differences in the specified
376 and actual material properties of the sawbones composite femurs [17] may present another
377 source of variability.

378 In this study, for consistency and to allow direct comparison of implant behaviour, all implants
379 (primary and revision) were implanted into healthy bone geometry which perfectly modelled the
380 inner shape of the implant. However, at the time of revision surgery, where stemmed implants
381 would typically be used, surgeons frequently encounter poor quality bone stock and large bony
382 defects. Such alterations to the underlying architecture of the bone may influence its response to
383 implantation [27, 46] and make long term survival of the prosthesis challenging. Additionally,
384 any alterations to the Young's modulus of the bone, through defects or disease, would likely
385 heavily influence inter-implant comparisons and substantially alter the levels of elastic
386 deformation experienced at the interface. Future studies should seek to understand how bone
387 quality (e.g. osteoarthritic v.s osteoporotic) and bony defects may influence motions and

deformations at the interface and how they might affect the trends presented here.

The models presented in this study are currently limited to predicting motion at the interface in the immediate post-implantation period. However, catastrophic loosening typically only occurs after millions of cycles [19]. On-gong work in our group aims to address both the time-dependent material response of bone [47] and its macroscopic yield behaviour [48], with a view to incorporate these aspects into future iterations of the models presented here, to allow predictions to extend to loosening and failure of the prosthesis.

4.1 Conclusion:

Experimentally verified finite element models can be used in a complementary manner to overcome many of the limitations traditionally associated with *in vitro* investigations of micromotion. These models are capable of providing insight into patterns of motion directly at the interface, as well as quantifying the levels of elastic deformation experienced by the bone for different implant geometries. Furthermore, the developed models have the ability to extend beyond the simplified *in vitro* loading conditions to characterise the influence of more physiologically realistic loads on the pattern and magnitude of motion at the interface. The outcomes of which have great relevance to the design and optimisation of orthopaedic implants and fixation strategies.

ACKNOWLEDGEMENTS:

Competing interests: None.

Funding: Financial support from the Lothian University Hospitals NHS Trust Brown and Ireland Estates Fund and The University of Edinburgh is gratefully acknowledged.

Ethical approval: Not required

REFERENCES:

1. AOA, *Annual Report*. 2011, Adelaide: Australian Orthopaedic Association National Joint Registry.
2. CJRR, *Hip and Knee Replacements in Canada 2008-2009 Annual Report* 2009, Ottawa: Canadian Joint Replacement Registry (CJRR).
3. NAR, *Norwegian Arthroplasty Register Annual Report*. 2010, Haukeland: Norwegian Arthroplasty Register.
4. NJR, *8th Annual Report.* National Joint Registry for England and Whales, 2011.
5. Sundberg, M., Lidgren, L., W-Dahl, A., and Robertsson, O., *The Swedish Knee Arthroplasty Register : Annual Report*. 2011. 62.
6. Abu-Amer, Y., Darwech, I., and Clohisy, J., *Aseptic loosening of total joint replacements: mechanisms underlying osteolysis and potential therapies.* Arthritis Research & Therapy, 2007. **9**(Suppl 1): p. S6.
7. Bahraminasab, M., Sahari, B.B., Edwards, K.L., Farahmand, F., Arumugam, M., and Hong, T.S., *Aseptic loosening of femoral components - A review of current and future trends in materials used.* Materials & Design, 2012. **42**: p. 459-470.
8. Kärrholm, J., *Roentgen stereophotogrammetry: Review of orthopedic applications.* Acta Orthopaedica, 1989. **60**(4): p. 491-503.
9. Nilsson, K.G. and Kärrholm, J., *RSA in the assessment of aseptic loosening.* Journal of Bone & Joint Surgery, British Volume, 1996. **78-B**(1): p. 1-3.
10. Nilsson, K.G., Karrholm, J., Ekelund, L., and Magnusson, P., *Evaluation of micromotion in cemented vs uncemented knee arthroplasty in osteoarthrosis and rheumatoid arthritis. Randomized study using roentgen stereophotogrammetric analysis.* The Journal of

Arthroplasty, 1991. **6**(3): p. 265-78.

11. Selvik, G., *Roentgen stereophotogrammetry.* Acta Orthopaedica, 1989. **60**(s232): p. 1-51.

12. Allen, M.J., *Functional micromechanics: moving beyond migration in evaluation of implant fixation.* J Am Acad Orthop Surg, 2011. **19**: p. 242-244.

13. Nilsson, K.G., Kärrholm, J., and Linder, L., *Femoral component migration in total knee arthroplasty: Randomized study comparing cemented and uncemented fixation of the Miller-Galante I design.* Journal of Orthopaedic Research, 1995. **13**(3): p. 347-356.

14. Ryd, L., *Micromotion in knee arthroplasty.* Acta Orthopaedica, 1986. **57**(s220): p. 3-80.

15. Abdul-Kadir, M.R., Hansen, U., Klabunde, R., Lucas, D., and Amis, A., *Finite element modelling of primary hip stem stability: The effect of interference fit.* Journal of Biomechanics, 2008. **41**(3): p. 587-594.

16. Chong, D.Y.R., Hansen, U.N., and Amis, A.A., *Analysis of bone–prosthesis interface micromotion for cementless tibial prosthesis fixation and the influence of loading conditions.* Journal of Biomechanics, 2010. **43**(6): p. 1074-1080.

17. Clarke, S., Phillips, A., and Bull, A., *Validation of FE Micromotions and Strains Around a Press-Fit Cup: Introducing a New Micromotion Measuring Technique.* Annals of Biomedical Engineering, 2012. **40**(7): p. 1586-1596.

18. Conlisk, N., Gray, H., Pankaj, P., and Howie, C.R., *The influence of stem length and fixation on initial femoral component stability in revision total knee replacement.* Bone Joint Res, 2012. **1**(11): p. 281-288.

19. Cristofolini, L., Affatato, S., Erani, P., Leardini, W., Tigani, D., and Viceconti, M., *Long-term implant-bone fixation of the femoral component in total knee replacement.* Proceedings of the Institution of Mechanical Engineers Part H-Journal of Engineering in

Medicine, 2008. **222**(H3): p. 319-331.

20. Cristofolini, L., Affatato, S., Erani, P., Tigani, D., and Viceconti, M., *Implant fixation in knee replacement: Preliminary in vitro comparison of ceramic and metal cemented femoral components.* Knee, 2009. **16**(2): p. 101-108.

21. Moran, M.F., *Computational and experimental assessment of total knee motion*, in *College of Health and Human Development*2005, The Pennsylvania State University. p. 187.

22. van Loon, C.J.M., Kyriazopoulos, A., Verdonschot, N., de Waal Malefijt, M.C., Huiskes, R., and Buma, P., *The role of femoral stem extension in total knee arthroplasty.* Clinical Orthopaedics and Related Research, 2000(378): p. 282-289.

23. Wackerhagen, A., Bodem, F., and Hopf, C., *The effect of cement fixation on initial micromotion of the femoral component in condylar knee replacement.* International Orthopaedics, 1992. **16**(1): p. 25-28.

24. Berzins, A., Sumner, D.R., Andriacchi, T.P., and Galante, J.O., *Stem curvature and load angle influence the initial relative bone-implant motion of cementless femoral stems.* Journal of Orthopaedic Research, 1993. **11**(5): p. 758-769.

25. Maher, S.A. and Prendergast, P.J., *Discriminating the loosening behaviour of cemented hip prostheses using measurements of migration and inducible displacement.* Journal of Biomechanics, 2002. **35**(2): p. 257-265.

26. Berahmani, S., Janssen, D., Wolfson, D., de Waal Malefijt, M., Fitzpatrick, C.K., Rullkoetter, P.J., and Verdonschot, N., *FE analysis of the effects of simplifications in experimental testing on micromotions of uncemented femoral knee implants.* Journal of Orthopaedic Research, 2016. **34**(5): p. 812-819.

27. Completo, A., Simões, J.A., and Fonseca, F., *Revision total knee arthroplasty: The influence of femoral stems in load sharing and stability.* The Knee, 2009. **16**(4): p. 275-279.

28. Tarala, M., Janssen, D., Telka, A., Waanders, D., and Verdonschot, N., *Experimental versus Computational Analysis of Micromotions at the Implant—Bone Interface.* Proceedings of the Institution of Mechanical Engineers, Part H: Journal of Engineering in Medicine, 2011. **225**(1): p. 8-15.

29. van der Ploeg, B., Tarala, M., Homminga, J., Janssen, D., Buma, P., and Verdonschot, N., *Toward a more realistic prediction of peri-prosthetic micromotions.* Journal of Orthopaedic Research, 2012. **30**(7): p. 1147-1154.

30. Bergmann G (ed.). *Charité Universitaetsmedizin* Berlin (2008) "OrthoLoad". Retrieved Jan. 10, 2010 from http://www.OrthoLoad.com

31. Bergmann, G., Bender, A., Graichen, F., Dymke, J., Rohlmann, A., Trepczynski, A., Heller, M.O., and Kutzner, I., *Standardized Loads Acting in Knee Implants.* PLoS ONE, 2014. **9**(1): p. e86035.

32. Taylor, S.J.G., Walker, P.S., Perry, J.S., Cannon, S.R., and Woledge, R., *The forces in the distal femur and the knee during walking and other activities measured by telemetry.* The Journal of Arthroplasty, 1998. **13**(4): p. 428-437.

33. Baldwin, M.A., Clary, C.W., Fitzpatrick, C.K., Deacy, J.S., Maletsky, L.P., and Rullkoetter, P.J., *Dynamic finite element knee simulation for evaluation of knee replacement mechanics.* Journal of Biomechanics, 2012. **45**(3): p. 474-483.

34. Bougherara, H., Zdero, R., Mahboob, Z., Dubov, A., Shah, S., and Schemitsch, E.H., *The biomechanics of a validated finite element model of stress shielding in a novel hybrid*

total knee replacement. Proceedings of the Institution of Mechanical Engineers. Part H: Journal of Engineering in Medicine, 2010. **224**(H10): p. 1209-1219.

35. Completo, A., Fonseca, F., and Simões, J.A., *Experimental validation of intact and implanted distal femur finite element models.* Journal of Biomechanics, 2007. **40**(11): p. 2467-2476.

36. Britton, J.R. and Prendergast, P.J., *Preclinical testing of femoral hip components: An experimental investigation with four prostheses.* Journal of Biomechanical Engineering-Transactions of the Asme, 2005. **127**(5): p. 872-880.

37. Monti, L., Cristofolini, L., and Viceconti, M., *Methods for Quantitative Analysis of the Primary Stability in Uncemented Hip Prostheses.* Artificial Organs, 1999. **23**(9): p. 851-859.

38. Gilbert, J.L., Bloomfeld, R.S., Lautenschlager, E.P., and Wixson, R.L., *A computer-based biomechanical analysis of the three-dimensional motion of cementless hip prostheses.* Journal of Biomechanics, 1992. **25**(4): p. 329-340.

39. Kuiper, J.H. and Huiskes, R., *Friction and stem stiffness affect dynamic interface motion in total hip replacement.* Journal of Orthopaedic Research, 1996. **14**(1): p. 36-43.

40. Rancourt, D., Shirazi-Adl, A., Drouin, G., and Paiement, G., *Friction properties of the interface between porous-surfaced metals and tibial cancellous bone.* Journal of Biomedical Materials Research, 1990. **24**(11): p. 1503-1519.

41. Viceconti, M., Muccini, R., Bernakiewicz, M., Baleani, M., and Cristofolini, L., *Large-sliding contact elements accurately predict levels of bone–implant micromotion relevant to osseointegration.* Journal of Biomechanics, 2000. **33**(12): p. 1611-1618.

42. Sawbones. *Biomechanical bones: 4th generation biomechanical composite femur*. 2008

29/08/2008; Available from: http://www.sawbones.com/products/product.aspx?1937.

43. Sumner, D.R., Berzins, A., Turner, T.M., Igloria, R., and Natarajan, R.N., *Initial in vitro stability of the tibial component in a canine model of cementless total knee replacement.* Journal of Biomechanics, 1994. **27**(7): p. 929-939.

44. Pettersen, S.H., Wik, T.S., and Skallerud, B., *Subject specific finite element analysis of implant stability for a cementless femoral stem.* Clinical Biomechanics, 2009. **24**(6): p. 480-487.

45. Taylor, M. and Tanner, K.E., *Fatigue failure of cancellous bone: a possible cause of implant migration and loosening.* J Bone Joint Surg Br, 1997. **79-B**(2): p. 181-182.

46. Conlisk, N., Howie, C.R., and Pankaj, P., *The role of complex clinical scenarios in the failure of modular components following revision total knee arthroplasty: A finite element study.* Journal of Orthopaedic Research, 2015. **33**(8): p. 1134 - 1141.

47. Xie, S., Manda, K., Wallace, R.J., Levrero-Florencio, F., Simpson, A.H.R.W., and Pankaj, P., *Time Dependent Behaviour of Trabecular Bone at Multiple Load Levels.* Annals of Biomedical Engineering, 2017: p. 1-8.

48. Levrero-Florencio, F., Margetts, L., Sales, E., Xie, S., Manda, K., and Pankaj, P., *Evaluating the macroscopic yield behaviour of trabecular bone using a nonlinear homogenisation approach.* Journal of the Mechanical Behavior of Biomedical Materials, 2016. **61**: p. 384-396.

LEGEND TO FIGURES:

Fig. 1: Rendered CAD models of a PS implant (top), a TS implant with short stem (middle) and a TS implant with long offset stem (bottom).

Fig. 2: a) image of *in vitro* setup and corresponding model, b) shows the virtual test rig where reference points represent the DVRT sensors (orange dots) and target spheres (blue dots). In this instance the target sphere attach back to the implant tool groove using coupling constraints and the DVRT attach to the bone at the approximate location of the sensor housing in the *in vitro* setup. The reference point about which all motions and rotations are calculated is indicated by the white dot, and c) detailed schematic of reference point position relative to the target spheres and sensors.

Fig. 3: *In vit*ro and computational results processing workflows.

Fig. 4: Comparison of the overall magnitude of relative displacement for both the FE and *in vitro* setups at 20° flexion, for a) uncemented and b) cemented scenarios. The upper and lower boundaries for fibrous tissue formation are indicated by the dashed orange line.

Fig. 5: a) anterior view, and b) posterior view of femoral component micromotion expressed as gap opening and shear micromotion in two orthogonal directions for a PS implanted femur (first column) and a TS implanted femur with short stem (second column) and a TS implanted femur with 4mm laterally offset stem (final column) under *in vitro* loading conditions.

Fig. 6: a) anterior view, and b) posterior view of femoral component micromotion expressed as gap opening and shear micromotion in two orthogonal directions for a PS implanted femur (first column) and a TS implanted femur with short stem (second column) and a TS implanted femur with 4mm laterally offset stem (final column) under physiological loading conditions.

Table 1: Summary of all cases examined at 20° flexion, with bone-implant interface conditions highlighted for both the *in vitro* tests and their corresponding finite element models.

	Interface conditions (*in vitro* tests)		**Interface conditions (FE models)**	
Implant type	**Cemented "tied"**	**Uncemented "frictional"**	**Tied**	**Frictional**
PS	All cemented		All tied	
		All frictional		All frictional
TS with short stem (12mm x 50mm)	All cemented		All tied	
		All frictional		All frictional
TS with long 4mm laterally offset stem (19mm x 150mm)	Implant only, stem frictional		Implant only tied, stem frictional	
		All frictional		All frictional

585 **Table 2:** Material properties applied to finite element model.

Component	Young's modulus E (MPa)	Poisson's ratio (v)
Cortical bone	16700	0.3
Cancellous bone	155	0.3
Femoral component (Co-Cr)	210000	0.3
Femoral stem (ti-6al-4v)	110000	0.3
Offset adapter	110000	0.3
Steel plate	210000	0.3
Tibial insert	463	0.46

586
587
588
589
590
591
592
593
594
595
596
597
598

Table 3: Forces used in the FE analyses for 20° flexion. Values were obtained from previous *in vivo* telemetric implant studies [30, 32], normalised in terms of body weight and then applied to the FE model for an assumed average body weight of 775N. Note: The sign of each component of force indicates its orientation in either the positive or negative direction in the knee joint coordinate system.

Component of force	**20°**
Medial Force Fm (N)	986
Lateral Force FL (N)	657
Medial Anterior-Posterior force APm (N)	-3
Lateral Anterior-Posterior force APl (N)	-3
Patella-Femoral Force PF (N)	567
Internal-External moment IE (Nmm)	-7029

Table 4: Absolute values of peak shear micromotion recorded at the interface for all implant types under both simplified and physiological loading conditions.

Implant	Cslip1 (µm)	Cslip2 (µm)
	Simplified loading	
PS	77.29	135.04
TSSS	84.45	115.98
TSLS	29.04	56.68
	Physiological loading	
PS	79.55	123.45
TSSS	94.15	100.17
TSLS	26.03	36.15

Table 5: Summary of the surface area calculated for each implant type and loading condition (simplified and physiological) at 20º flexion for six different bands of shear micro motion (0 – 20μm, 20 – 40μm, 40 – 60μm, 60 – 80μm, 80 – 100μm and 100 – 150μm). The values in brackets represent the area expressed as a percentage of the total area in contact at the interface.

		0 – 20μm (mm^2)	20 – 40μm (mm^2)	40 – 60μm (mm^2)	60 – 80μm (mm^2)	80 – 100μm (mm^2)	100 – 150μm (mm^2)
				Simplified loading			
PS	Cslip 1	8806.77 (95.02)	404.59 (4.37)	52.65 (0.57)	4.42 (0.05)	0.00	0.00
	Cslip 2	8503.12 (91.74)	312.37 (3.37)	230.63 (2.49)	106.95 (1.15)	53.12 (0.57)	62.24 (0.67)
TSSS	Cslip 1	10376.32 (95.03)	379.32 (3.50)	68.65 (0.63)	14.86 (0.14)	0.00	0.00
	Cslip 2	10216.26 (94.25)	301.22 (2.78)	171.57 (1.58)	90.88 (0.84)	43.96 (0.41)	15.27 (0.14)
TSLS	Cslip 1	10772.31 (99.82)	19.04 (0.18)	0.00	0.00	0.00	0.00
	Cslip 2	10577.17 (98.01)	144.12 (1.34)	70.07 (0.65)	0.00	0.00	0.00
				Physiological loading			
PS	Cslip 1	8541.07 (92.15)	505.62 (5.46)	177.62 (1.92)	44.11 (0.48)	0.00	0.00
	Cslip 2	8136.83 (87.79)	535.55 (5.78)	411.45 (4.44)	166.83 (1.80)	14.72 (0.16)	3.05 (0.03)
TSSS	Cslip 1	10377.28 (95.74)	197.72 (1.82)	130.98 (1.21)	126.15 (1.16)	7.03 (0.06)	0.00
	Cslip 2	9814.52 (90.55)	521.05 (4.81)	394.17 (3.64)	99.21 (0.92)	10.20 (0.09)	0.00
TSLS	Cslip 1	10686.47 (99.03)	105.01 (0.97)	0.00	0.00	0.00	0.00
	Cslip 2	10699.10 (99.14)	92.38 (0.86)	0.00	0.00	0.00	0.00

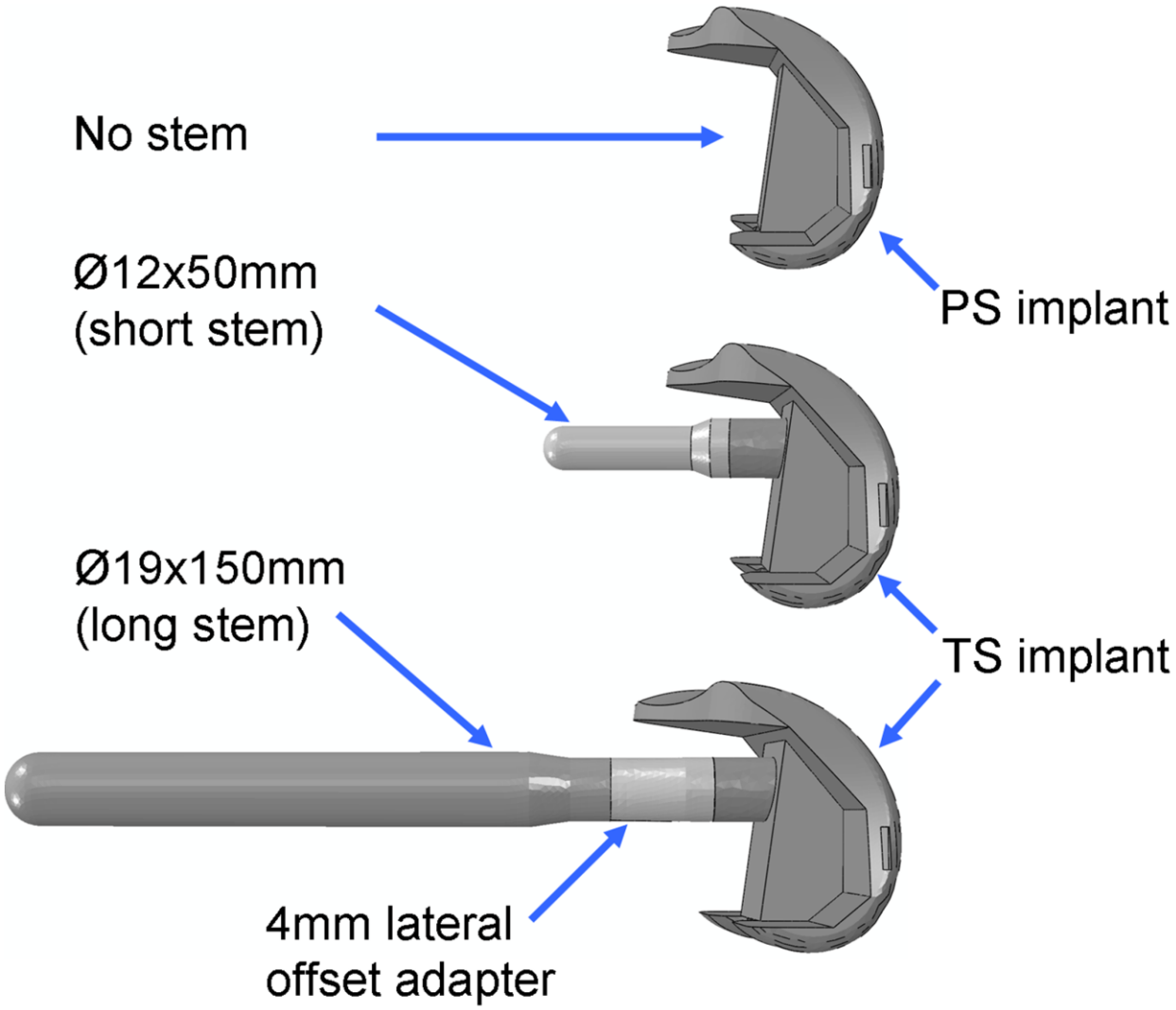
No stem
Ø12x50mm
(short stem)
Ø19x150mm
(long stem)
4mm lateral
offset adapter
PS implant
TS implant

635

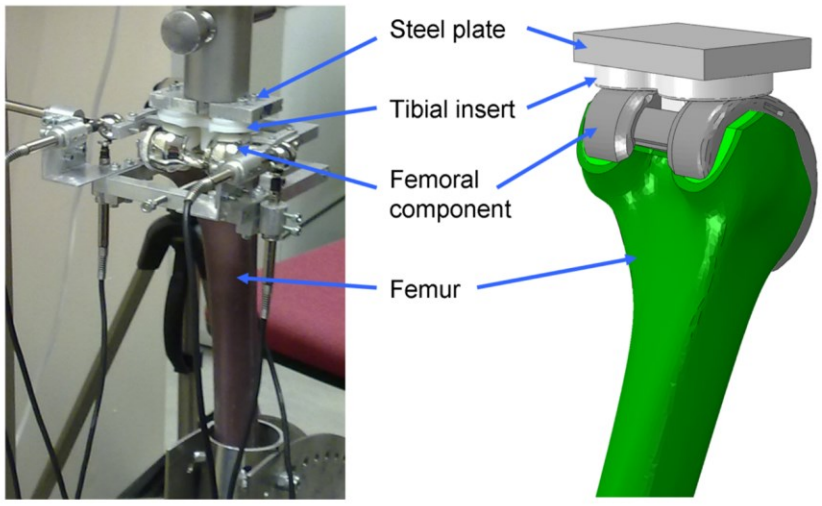
Steel plate
Tibial insert
Femoral component
Femur

a)

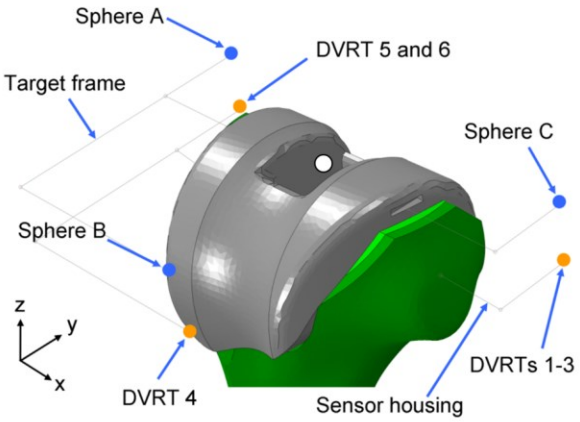
Sphere A
DVRT 5 and 6
Target frame
Sphere C
Sphere B
z
y
x
DVRT 4
DVRTs 1-3
Sensor housing

b)

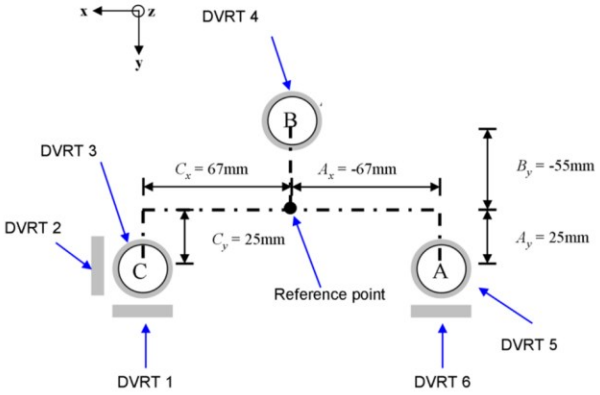
x
z
y
DVRT 4
B
DVRT 3
C_x = 67mm
A_x = -67mm
B_y = -55mm
DVRT 2
C_y = 25mm
A_y = 25mm
C
A
Reference point
DVRT 5
DVRT 1
DVRT 6

c)

636

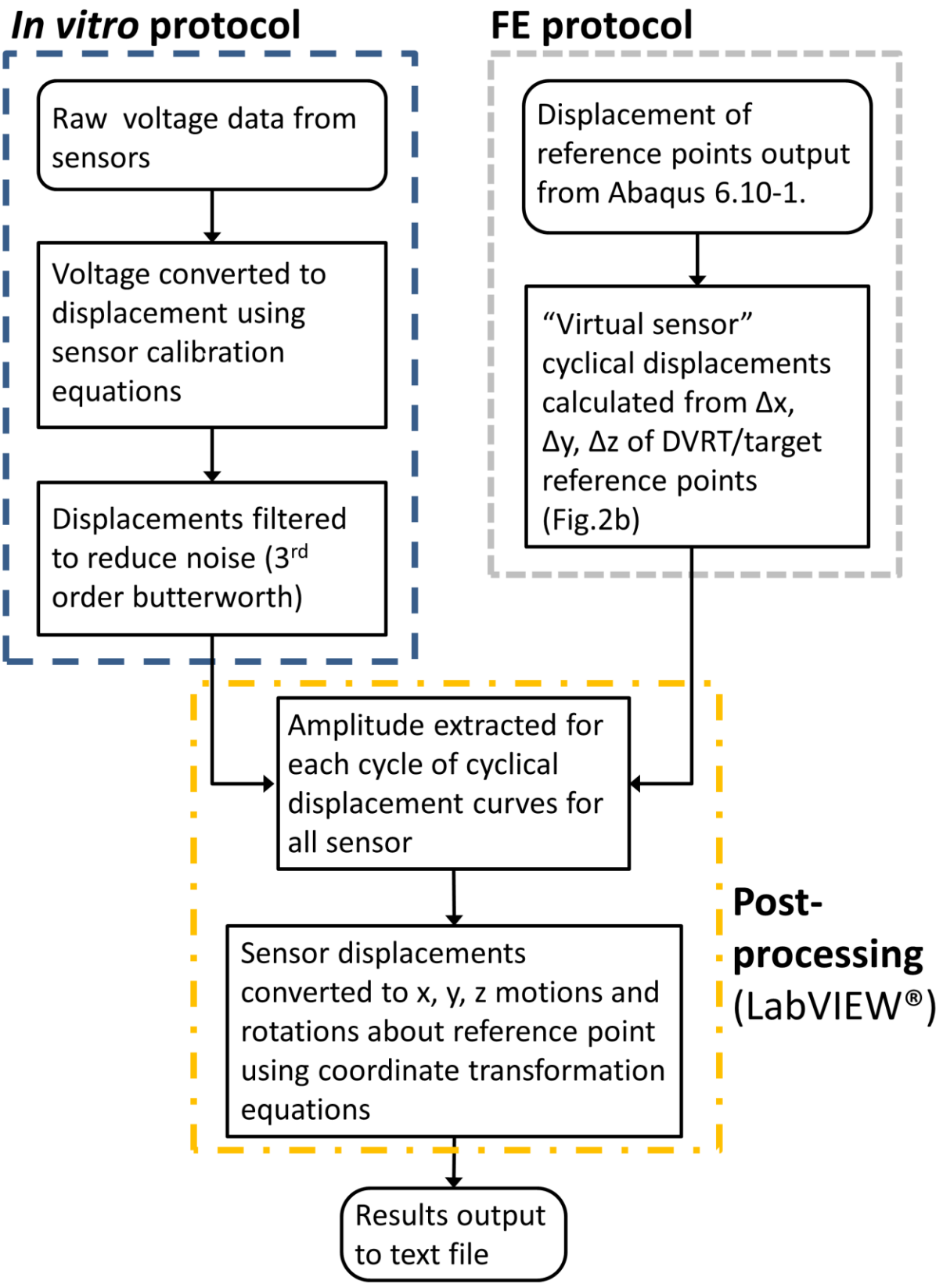
In vitro protocol
Raw voltage data from sensors
Voltage converted to displacement using sensor calibration equations
Displacements filtered to reduce noise (3rd order butterworth)
FE protocol
Displacement of reference points output from Abaqus 6.10-1.
"Virtual sensor" cyclical displacements calculated from Δx, Δy, Δz of DVRT/target reference points (Fig.2b)
Amplitude extracted for each cycle of cyclical displacement curves for all sensor
Sensor displacements converted to x, y, z motions and rotations about reference point using coordinate transformation equations
Post-processing (LabVIEW®)
Results output to text file

637

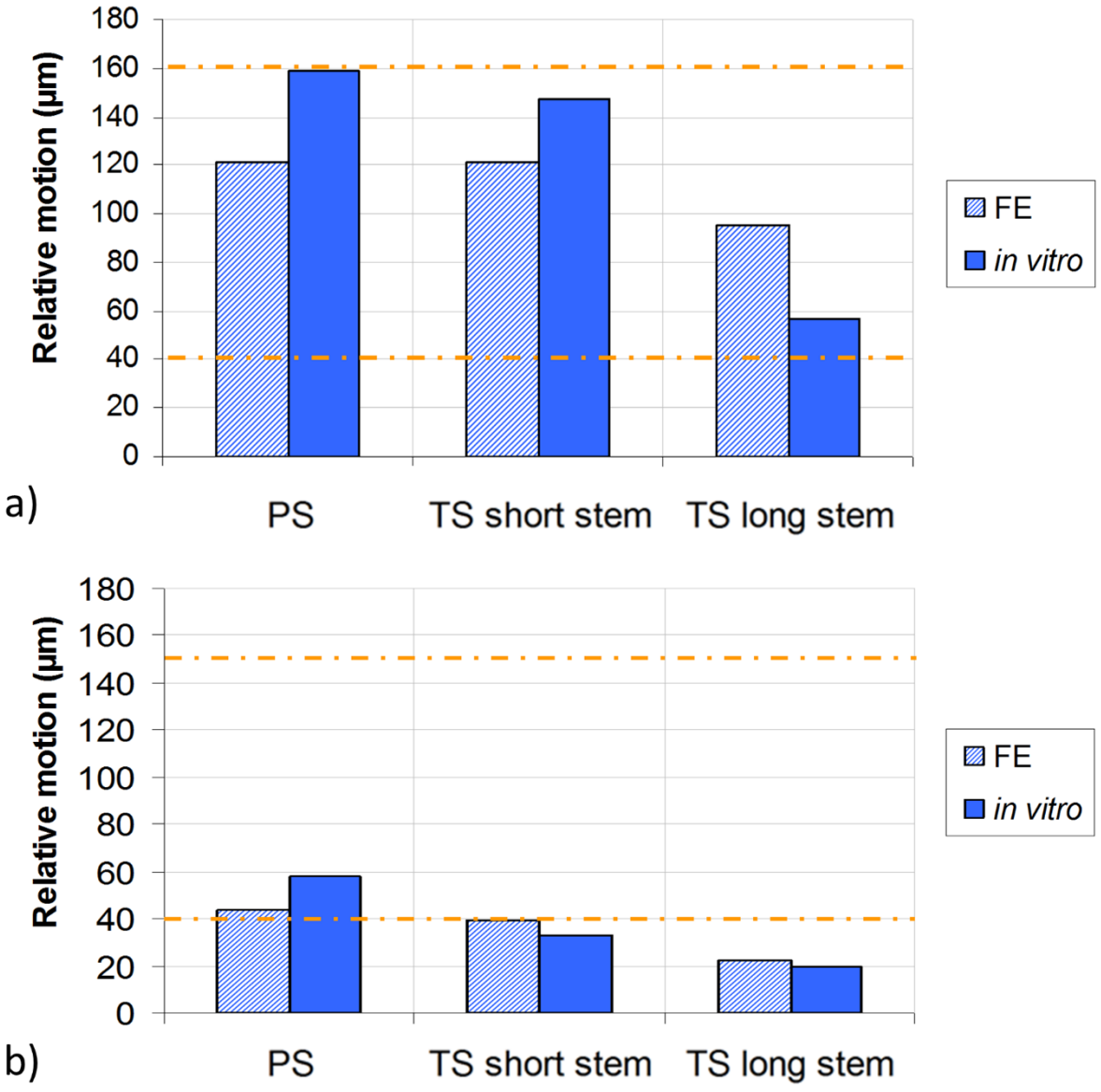
Relative motion (µm)
180
160
140
120
100
80
60
40
20
0
FE
in vitro
PS
TS short stem
TS long stem
a)
Relative motion (µm)
180
160
140
120
100
80
60
40
20
0
FE
in vitro
PS
TS short stem
TS long stem
b)

638

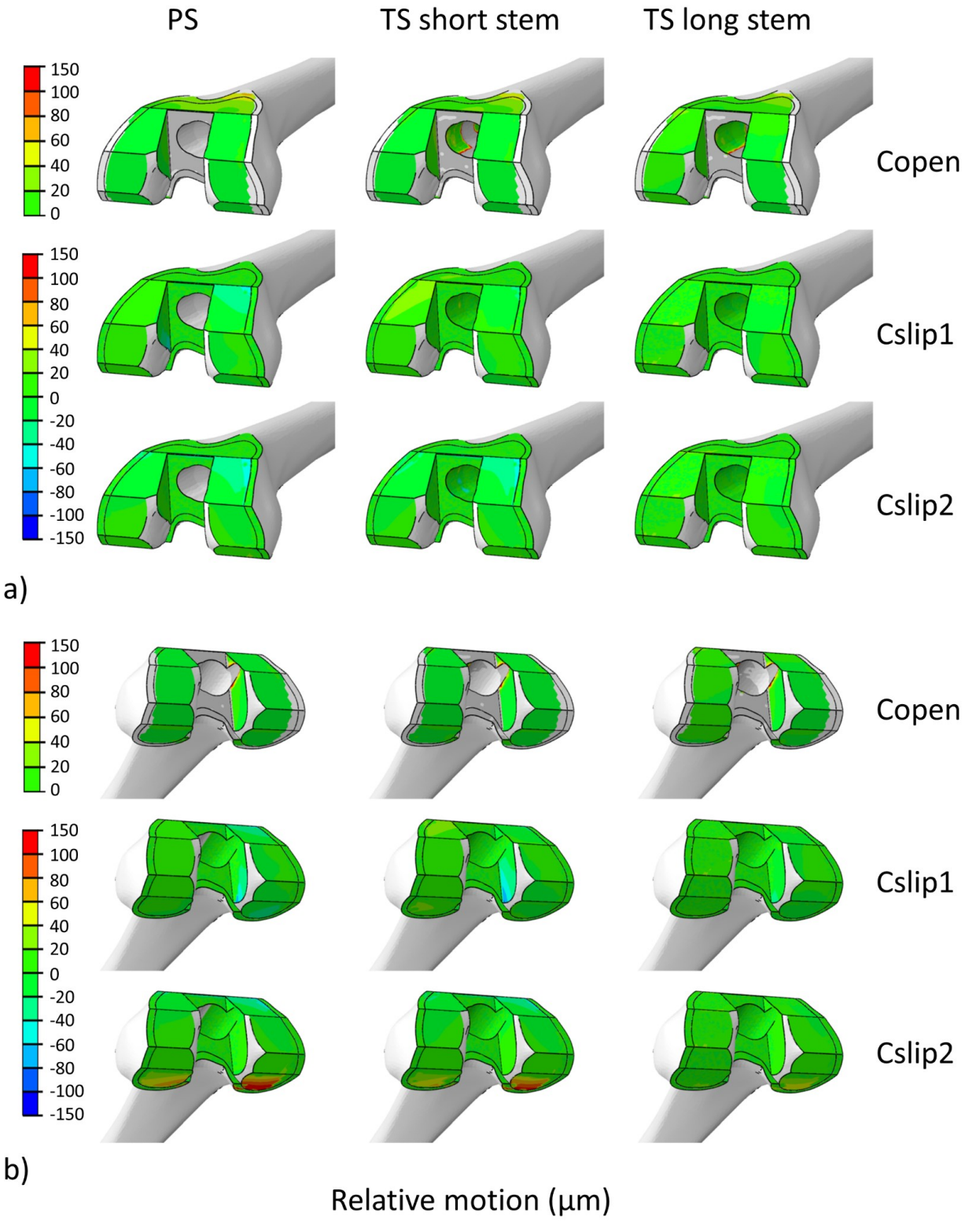
PS
TS short stem
TS long stem
150
100
80
60
40
20
0
-20
-40
-60
-80
-100
-150
Copen
Cslip1
Cslip2
a)
b)
Relative motion (µm)

639

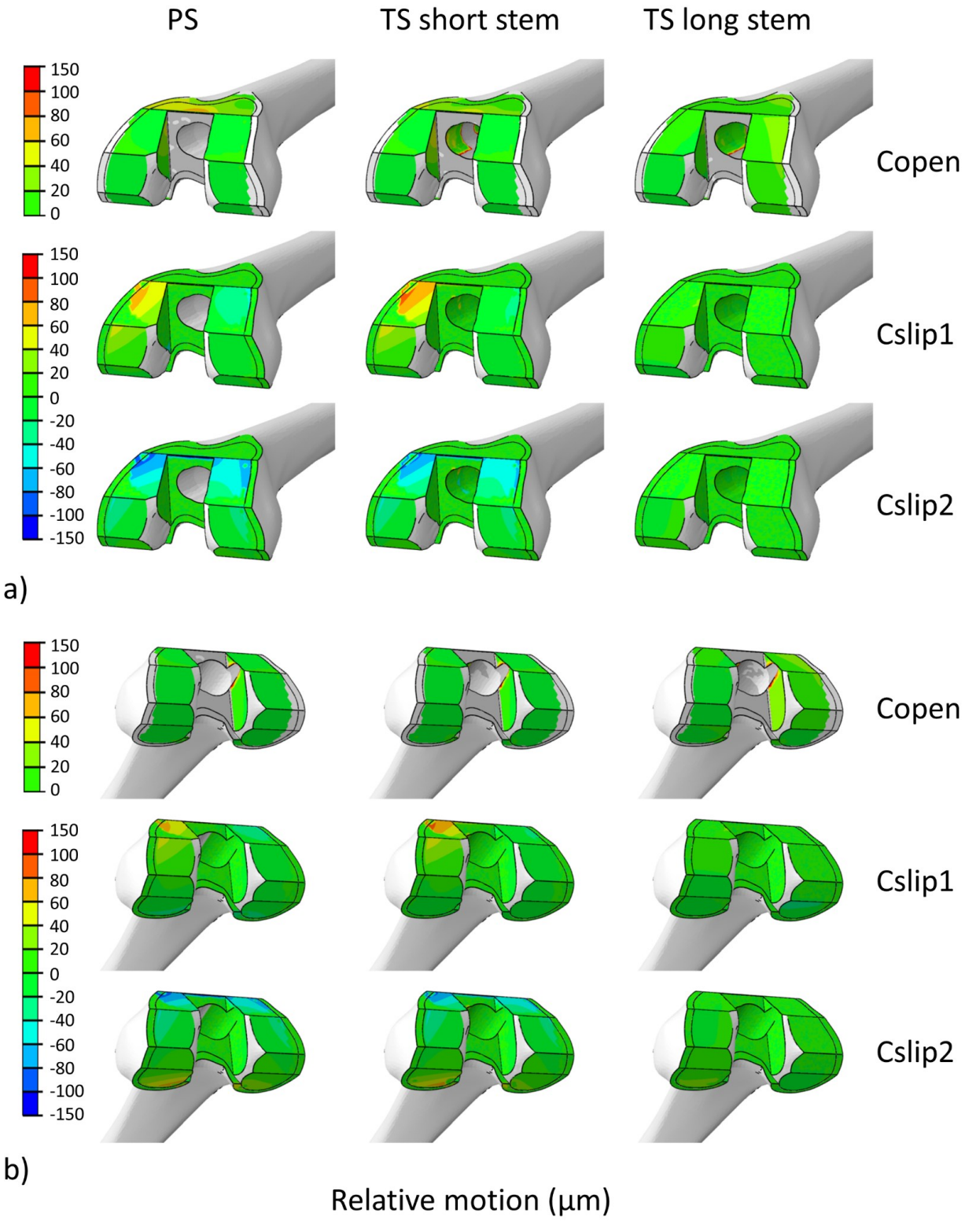
PS
TS short stem
TS long stem
150
100
80
60
40
20
0
-20
-40
-60
-80
-100
-150
Copen
Cslip1
Cslip2
a)
b)
Relative motion (µm)

640